2024 6th International Conference on Reconfigurable Mechanisms and Robots (ReMAR)
June 24-27, 2024. Chicago, IL, USA

A Multi-Facet-Effector Soft Robot in Polyhedral Configuration for Multidirectional Function Reuse

Yige Wu, Xiaohuang Liu, Shaowu Tang, Sicong Liu*, *Member, IEEE,* Juan Yi, *Member, IEEE,* Zheng Wang, *Senior Member, IEEE,* and Jian S Dai*, *Fellow, IEEE*

2024 6th International Conference on Reconfigurable Mechanisms and Robots (ReMAR) | 979-8-3503-9596-9/24/$31.00 ©2024 IEEE | DOI: 10.1109/REMAR61031.2024.10619986

***Abstract*—Soft robots are known for their adaptability in unstructured environments, providing the flexibility required for complex tasks. Existing designs are often tailored explicitly for particular functionalities, lacking the ability to accommodate diverse task requirements. To address the challenges, we propose an innovative approach employing Multi-Facet-Effector (MFE) in the design of a soft robot. The MFE functions both as a gulp gripper (MFG) and a parallel arm (MFA), achieving versatile capabilities without the need for intricate and specific designs. Three Soft-Bellowed Actuators (SBAs) constitute the identical regular triangle in each facet of an octahedral-shaped configuration. When working as the MFG, the robot exhibits the capability to grasp objects within a diameter range of 36.3-109.1 mm, with the maximum holding force up to 7 N. This gripping stability extends to objects of various shapes, rigidities, and weights. When working as the MFA, experimental results reveal six degrees of freedom (DOFs) at the top pose, with five DOFs exhibiting symmetric behaviors. The translational distance along the X and Y axes reaches 42.2 mm, while the Z-axis spans from -67.1 to 29.4 mm. Unidirectional rotation angles around the X, Y, and Z axes are 27.2°, 30.7°, and 35.7°, respectively. A kinematic model for the MFA movements is established and validated through experiments. The inherent characteristic of identical motion and functionality across each facet of the MFE soft robot allows for the efficient utilization of repetitive configurations. Through coordinated actions among the facet-effectors, the robot is capable of executing a variety of tasks in three-dimensional (3D) space, such as multi-facet manipulations and climbing on complex spatial terrains.**

I. Introduction

Soft robots have attracted significant attention in recent years [1, 2] thanks to their inherent compliance and deformability. These characteristics enable soft robots to exhibit remarkable adaptability across various applications, such as wearable devices, underwater manipulations, and dexterous grasping [3-6]. Their unique features empower effective interactions under simple control, facilitating the execution of a wide range of tasks. Consequently, researchers are increasingly focusing on utilizing soft robots to tackle challenges in unstructured environments. Some studies explore adaptive strategies for bio-inspired interactive soft robots in humid environments [7], which typically require capabilities for interacting with the environment, such as grasping, manipulation, and locomotion.

The utilization of limbs or tentacles for grasping or manipulating objects is a fundamental mode of interaction between many organisms and their environment [8, 9], often actuated by pneumatic systems [10]. Grasping involves picking up and holding objects free from external disturbances, while manipulation entails applying forces to objects, leading to their rotation and displacement relative to the reference frame of the robotic hand [11]. The addition of degrees of freedom (DOF) enables grippers to possess manipulation capabilities [12]. Studies have reported on flexible-axis-driven soft robotic grippers capable of simultaneously grasping and manually manipulating bottle caps [13]. Additionally, some soft robots leverage adhesion to move or stay on various surfaces. Recent developments have showcased octopus-like soft arms with capabilities such as reaching, grasping, and interacting [14].

In terms of locomotion, various motion strategies have been explored using soft robots. Simultaneously, the introduction of reconfigurable technology further enhances the adaptability and versatility of robots [15, 16]. Many organisms, including various spiders and caterpillars, alter their shapes to modify gaits and adapt to different surroundings [17, 18]. The utilization of soft pneumatic actuators capable of undergoing extensive deformations under pressurization enables motion along the exterior of a cylindrical object, as exemplified by soft robotic climbers for pipes [19, 20]. Researchers have also applied the Stewart platform to soft robotics, endowing the soft robotic arm with flexible six DOFs in motion [21, 22].

Integrating grasping and locomotion functionalities into soft robotic platforms presents an intriguing perspective. Inspired by ants, a study has utilized mandibles and neck joints to lift objects and legs to carry loads [23]. Additionally, underwater octopus robots have been developed, with different arms serving distinct purposes such as elongation, grasping, and locomotion [24]. Nevertheless, these designs often rely on distinct structures to achieve different functionalities [25]. Consequently, researchers are increasingly exploring the creation of multifunctional soft robots with identical structures, broadening their potential applications. For instance, tetrahedral soft robots combine motion and grasping capabilities for object transport [26], while wormlike robots enable continuous transportation inside the bio-inspired body cavity [27]. Moreover, mesh rolling and stacking soft robots can perform various tasks [28], and robots integrated with disassembly structures can move, support, and lift objects [29].

* This work was partly supported by the National Key R&D Program of China (Grant No. 2022YFB4701200), Shenzhen Science and Technology Program Grant JCYJ20220530114615034 and JCYJ20220818100417038, Guangdong Basic and Applied Basic Research Foundation Grant 2021A1515110658.

Yige Wu, Xiaohuang Liu, Shaowu Tang, Sicong Liu, Juan Yi, Zheng Wang, and Jian S Dai are with the Department of Mechanical and Energy Engineering, Southern University of Science and Technology, Shenzhen 518000, China (Corresponding Authors: Sicong Liu, Jian S Dai) (e-mail: 12232329@mail.sustech.edu.cn, 13232404@mail.sustech.edu.cn, 12232306@mail.sustech.edu.cn, liusc@sustech.edu.cn; yij3@sustech.edu.cn; wangz@sustech.edu.cn).

However, the current research predominantly emphasizes robots with designs for specific applications, often tailored to particular functional orientations.

In this work, a Multi-Facet-Effector (MFE) soft robot with a highly symmetric configuration is proposed. This concept introduces uniformly located effectors at each facet of a polyhedron, comprising soft actuators arranged in a regular polygon. By leveraging the uniform motion and functionality of each effector facet unit, a variety of functions can be achieved under simple control.

This paper contributes by proposing a Multi-Facet-Effector (MFE) soft robotic design featuring regular polygonal effectors uniformly distributed on each facet of a polyhedral configuration. This design allows the robot to function versatilely as both a gulp gripper (MFG) and a parallel arm (MFA). The design, modeling, and control strategy for an octahedral MFE robot are presented, and theoretical results are validated through experiments, demonstrating the robot's functionalities.

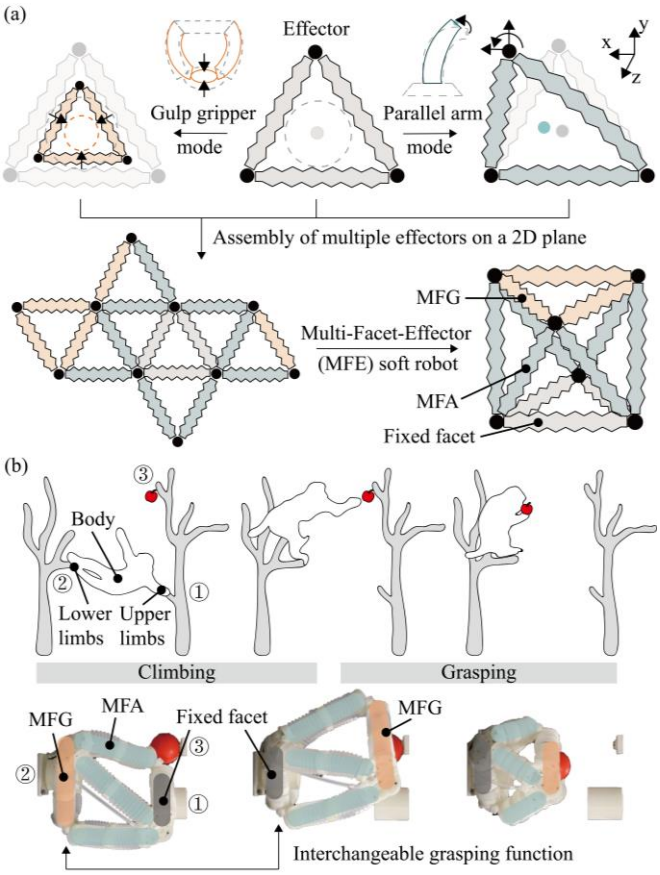

Figure 1. The concept of Multi-Facet-Effector (MFE) design. (a) A facet-effector consists of three identical soft actuators forming a 2D triangle configuration that generates two functional modes: the gulp gripper and the parallel arm. The facet-effectors are assembled into a multi-facet-effectors robot with an octahedra structure. (b) The primates use upper and lower limbs in an alternating fashion to grab and navigate between tree trunks, which inspires the MFE soft robot to accomplish continuous grasping and climbing by the coordinate movements of multi-facet-effectors.

Section II of this paper explores the concept, design, and implementation of MFE in a soft robot. Section III introduces the modeling and control of an octahedral MFE structure. Section IV showcases the robot's performance in two modes in experiments and demonstrations. Section V concludes the work.

II. Concept and Design

Functional reuse endows organisms with robust locomotive capabilities in nature. The soft robotic structural design is inspired by the interchangeable grasping function of the upper and lower limbs of primates, allowing the arms to hook onto one tree branch while the feet hook onto another when navigating through trees. Alternating between upper and lower limbs, the animal can achieve seamless and consecutive movements through randomly located tree branches. Fig. 1(a) shows a scalable two-dimensional (2D) triangle that can enlarge and contract and be conceptualized as a facet-effector. The effector can function as a gulp gripper when the actuators elongate and contract together and as a parallel arm when the actuators deform coordinately. By implementing the facet-effectors as the discrete surfaces of a polyhedral, this concept expands to constitute 3D configurations that lead to the MFE robot. Every facet-effector possesses two functional modes. Thus, the MFE robot can function versatilely as both a gulp gripper (MFG) and a parallel arm (MFA). Through the repositioning of grippers and arms, the robot achieves functions like climbing or performing operations in 3D space using the interchangeable functionality of the multi-facet-effectors (Fig. 1(b)).

A. Soft-Bellowed Actuator

As illustrated in Fig. 2, a soft-bellowed actuator (SBA) is an actuator comprising two bellows, a bellow connector, and two end caps, offering linear expansion and contraction capabilities. The bellows determine the deformability, while the bellow connector works as the reinforcement for enhanced stiffness. Various actuators can be designed based on functional requirements, with parameters such as dihedral angle, thickness, and material being crucial considerations.

The bellows are selected based on validated design parameters from previous studies [30, 31]. The parameters of the actuator are listed in Table I, offering enough motion range and flexibility for the effector. The bellows are low-cost and mass-produced using molded plastic, and the other components are produced by 3D printing. The bellows, connector, and end caps are bonded using hot melt adhesive.

A silicone layer is added to the bellow connector to increase contact friction. The end caps are designed to connect directly to the air tube, and it has preset holes for simple assembly and maintenance using screws and nuts.

B. Facet-Effector Design

To achieve multi-DOF mobility in a closed-loop form, we choose an equilateral triangle design to construct the facet-effector unit. Three SBAs are connected head-to-toe with 120° angles in between. In the planar state, when one SBA is fixed, the length variations in the other two actuators generate 3-DOF movements (Fig. 1(a)) of the opposite vertex, including

two in-plane translations and one rotation. The layout possesses the characteristic of distributing forces uniformly, which can obtain stable interactions with the external environment.

The effector can serve as a gripper or an arm by purposefully controlling the input pressure. The gripping diameter is $d_{SGA} = \frac{\sqrt{3}}{3}(l_{SBA} + 2a) - d_{SBA}$. The modular and easily assembled architecture allows for the quick creation of various configurations that are composed of triangles on each face. The predominant use of soft materials enables the robot to safely interact with fragile objects or biological organisms, adapting to unknown and unstructured environments. This structural design facilitates large-scale deformations from a 2D sheet-like design, benefiting application scenarios that need maneuverability in confined spaces.

C. MFE Soft Robot

When expanding into 3D space, unlike the state-of-the-art tetrahedron-configuration robots [26, 32, 33], we choose the configuration of a regular octahedron for providing an adequate number of facets, which offers the needed flexibility without introducing excessive complexity in the body. The structure enhances the robot's mobility in complex environments, thereby expanding its potential applications. This design endows the robot with eight facet effectors and twelve SBAs. Different facet-effectors can switch function modes during various operations.

The configuration possesses sufficient flexibility and versatility, not only due to the presence of multiple facets but also because the central position of one effector can change under the influence of other effectors. By adjusting input pressure, an actuator on one facet can function as a gripper while actuators on other facets can act as arms simultaneously, thus achieving a combination of mobility and manipulation.

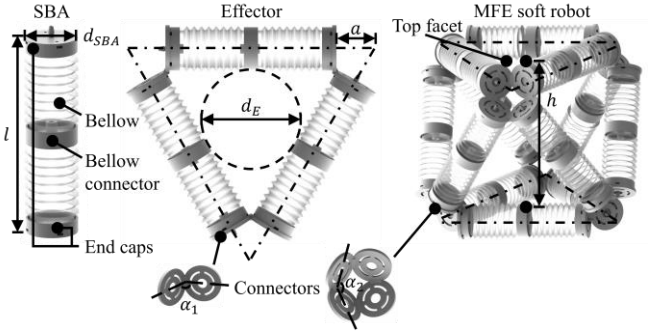

Figure 2. Design of SBA, 2D facet-effector, and the MFE soft robot in an octahedral configuration.

TABLE I. GEOMETRIC PARAMETERS OF THE DESIGN

d_{SBA}	Diameter of the actuator	36.3mm
l	Static length of the actuator	133.0mm
a	Distance between the center of two caps	32.6mm
α_1	Angle between the left and right caps	120°
α_2	Angle between the up and down caps	120°
d_E	Static inner diameter of the effector	78.1mm
h	Static distance between parallel faces	161.8mm

III. MODELING AND CONTROL

The kinematics model is built to obtain the relationship between the length of SBAs and the movement of the top facet, as shown in Fig. 3(a), which depicts the schematic diagram of the model. The deformations of the SBAs are determined by the input pressure. The initial height of the robot is $h = \frac{\sqrt{6}}{3}(l + 2a)$. It is assumed that the SBAs of the upper and lower effectors denoted as $l_1 - l_3$ and $l_{10} - l_{12}$ respectively, are equal in length and fixed. The original lengths of $l_1 - l_{12}$ are designated as l_0. Defining the direction parallel to l_{10} as the X-axis, perpendicular to l_{10} as the Y-axis, and vertically upward as the Z-axis, originating from point O.

The geometry diagrams of six DOFs are illustrated in Fig. 3(b). The known condition of the input pressures corresponds to the lengths $l_4 - l_9$, and the movements are designated as Δx, Δy, Δz for translations, and α, β, γ for rotations, respectively. The derivation of the forward kinematics model is presented. Suppose $\mathrm{A}(a_x, a_y, a_z)$ becomes point $\mathrm{A}'(a'_x, a'_y, a'_z)$ after translating along the X-axis. Focus on ΔAFD and ΔA′FD,

$$a_x = 0,\ a'_x = \sqrt{l_4^2 - \left(\frac{2S_{\Delta \mathrm{A'FD}}}{l_0}\right)^2} - \frac{l_0}{2}, \tag{1}$$

where $S_{\Delta \mathrm{A'FD}} = f(l_4, l_5) = \sqrt{p(p - l_0)(p - l_4)(p - l_5)}$, $p = \frac{l_0 + l_4 + l_5}{2}$. Thus, translation X is simplified to,

$$\Delta x = a'_x - a_x = \frac{l_4^2 - l_5^2}{2l_0}. \tag{2}$$

Suppose P and Q are the midpoints of BC and DF respectively, $P(p_x, p_y, p_z)$ becomes point $P'(p'_x, p'_y, p'_z)$ after translating along the Y-axis. Focus on ΔPQE and ΔP′QE,

$$p_y = -\frac{\sqrt{3}}{6}l_0,\ p'_y = \sqrt{l_{P'Q}^2 - \left(\frac{2S_{\Delta P'QE}}{l_{\mathrm{QE}}}\right)^2} - \frac{l_{QE}}{2}, \tag{3}$$

where $l_{\mathrm{P'Q}} = l_{\mathrm{B'D}} = l_6$, $l_{\mathrm{P'E}} = \sqrt{l_7^2 - \left(\frac{l_0}{2}\right)^2}$, $l_{\mathrm{QE}} = \frac{\sqrt{3}}{2}l_0$, and $S_{\Delta \mathrm{P'QE}} = f(l_6, l_7) = \sqrt{p(p - l_{\mathrm{QE}})(p - l_{\mathrm{P'Q}})(p - l_{\mathrm{P'E}})}$, $p = \frac{l_{\mathrm{QE}} + l_{\mathrm{P'Q}} + l_{\mathrm{P'E}}}{2}$. Translation Y simplifies to,

$$\Delta y = p'_y - p_y = \frac{l_6^2 - l_7^2}{\sqrt{3}l_0}. \tag{4}$$

Suppose M is the perpendicular projection of A' onto the base. Focus on ΔAMQ and ΔA′MQ, the length of MQ remains unchanged,

$$a_z = \frac{\sqrt{6}}{3}l_0, a'_z = \sqrt{l_{A'Q}^2 - l_{\mathrm{MQ}}^2}, \tag{5}$$

where $l_{\mathrm{MQ}} = \sqrt{l_{\mathrm{AQ}}^2 - l_{\mathrm{AM}}^2} = \frac{\sqrt{3}}{6}l_0$ and $l_{\mathrm{A'Q}} = \sqrt{l_4^2 - \left(\frac{l_0}{2}\right)^2}$. Translation Z simplifies to,

$$\Delta z = a'_z - a_z = \sqrt{l_4^2 - \frac{1}{3}l_0^2} - \frac{\sqrt{6}}{3}l_0. \tag{6}$$

Suppose N is the intersection of A'P' and QE, according to the Piecewise Constant Curvature, P'N = EN and A'N = QN. Therefore, Rotation X can be obtained as,

$$\Delta\alpha = \frac{\mathrm{P'E-A'Q}}{\frac{\sqrt{3}}{2}l_0} = \frac{\sqrt{l_4^2-\left(\frac{l_0}{2}\right)^2}-\sqrt{l_7^2-\left(\frac{l_0}{2}\right)^2}}{\frac{\sqrt{3}}{2}l_0}. \quad (7)$$

Similarly, Rotation Y can be obtained as,

$$\Delta\beta = \frac{\mathrm{B'D-C'F}}{\frac{\sqrt{3}}{2}l_0} = \frac{l_6-l_9}{\frac{\sqrt{3}}{2}l_0}. \quad (8)$$

Suppose h is the distance between parallel faces, and r is the radius of the circumcircle of ΔABC, which remains unchanged,

$$\begin{cases} {a'_x}^2 + {a'_y}^2 = r^2, \\ (a'_x - f_x)^2 + \left(a'_y - f_y\right)^2 + (h)^2 = l_4^2, \\ (a'_x - d_x)^2 + \left(a'_y - d_y\right)^2 + (h)^2 = l_5^2, \end{cases} \quad (9)$$

where $r = \frac{l_0}{\sqrt{3}}$, $d_x - f_x = l_0, d_y - f_y = 0$. Rotation Z simplifies to,

$$\theta_z = \arccos\sqrt{1-\left(\frac{l_4^2-l_5^2}{2*l_0*r}\right)^2}. \quad (10)$$

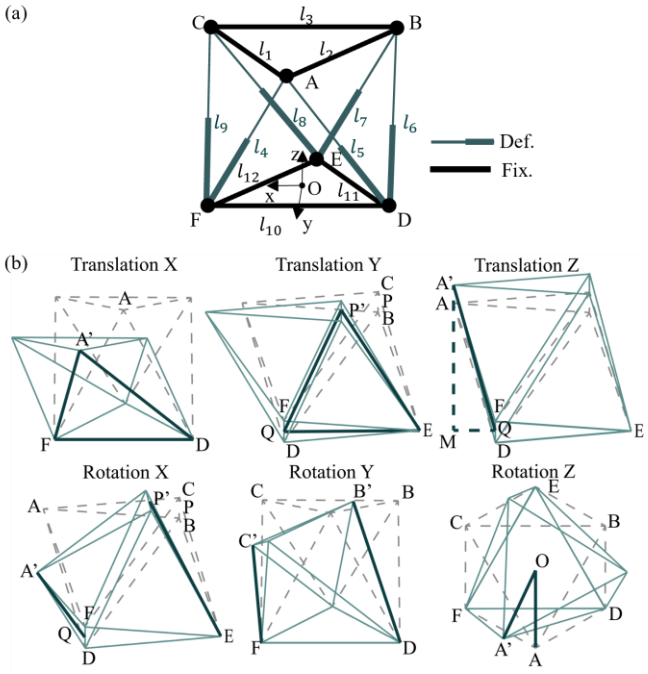

Figure 3. Modeling of the 6-DOF movements. (a) The model schematic where the top and bottom facets are fixed, with SBAs in the body capable of deformation. (b) Geometry diagram of six DOFs.

IV. Experiments

Experiments are carried out to explore the mechanical characteristics of the actuator and the performance of the robot, which functions as MFG and MFA.

A. Experimental Setup and Methodology

An integrated pneumatic actuation system, as shown in Fig. 4(a), is constructed to facilitate experiments involving pneumatic input and data acquisition. The setup contains a booster pump (KZP-PF, kamoer Inc.) and a vacuum pump (KVP300-KB, kamoer Inc.) to provide the pneumatic supply. The microcontroller (STM32F103C8T6, ST Microelectronics Inc.) regulates the 16 pneumatic channels through solenoid valves. Each channel is equipped with a pressure sensor (XGZP6857A, CFSensor Inc.). The system also captures data from external sensors: a laser sensor (HG-C1200, Panasonic Inc.) for displacement, a one-dimensional force sensor (DYMH-103, DAYSENSOR Inc.), a torque sensor (DYJN-104, DAYSENSOR Inc.), and an IMU (JY61, WitMotion Inc.) for angular measurements. Data is collected through the ADC module and serial port and subsequently processed using MATLAB (R2020b, MathWorks).

In the experiments, pressurized SBAs are labeled in red, and depressurized SBAs are labeled in blue, and non-pressurized SBAs are marked as blank, controlled by the integrated experimental setup. Control system logic is shown in Fig. 4(b).

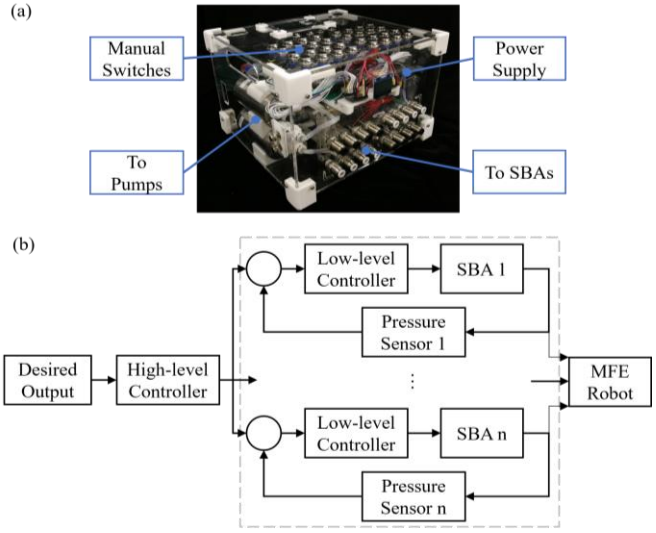

Figure 4. The control system. (a) A hardware system that can provide a stable pressure supply for 16 channels of suction and inflation and read sensor data. (b) Control system logic.

B. Actuator Characterization

The apparatus shown in Fig. 5(a) is designed to measure the displacement of SBA and output force under pneumatic input. Slow pressure input induces SBA movement along the slide rail, and pressure sensor and laser sensor data are recorded and plotted in Fig. 5(a). Due to hysteresis effects, deviations are observed between the extension and contraction curves. The actuator undergoes repeat experiments, and the averaged data within the practical working range is fitted by segmented linear functions with R^2=0.996, which is reliable and can simplify subsequent calculations for the model. The relation is expressed by the following equations,

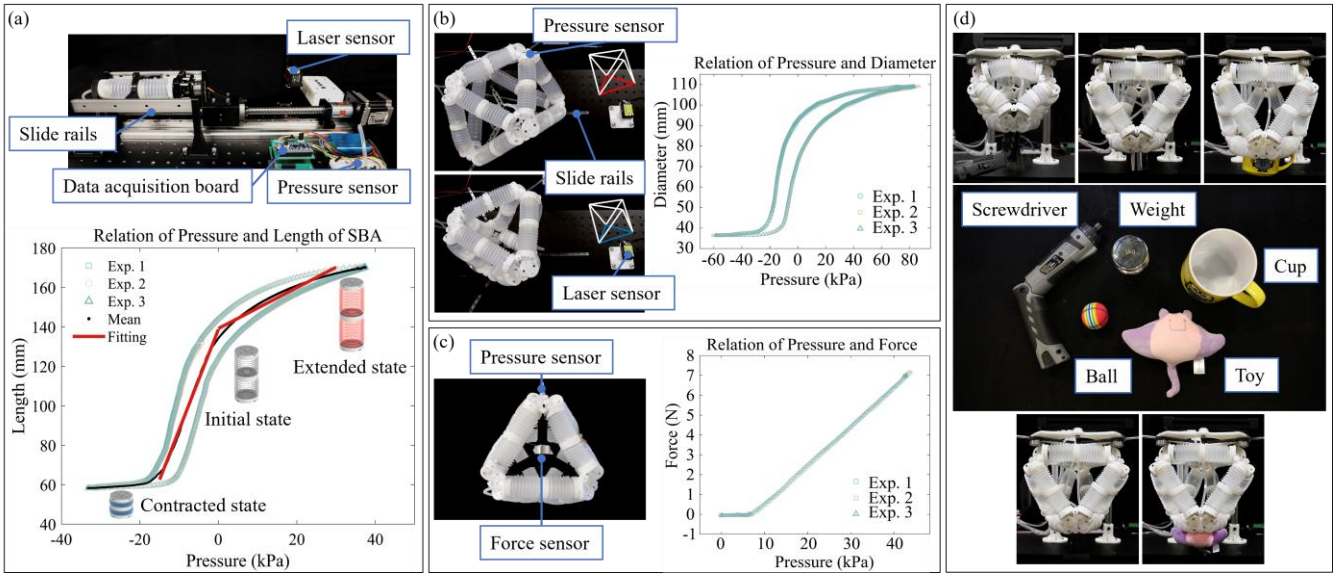

Figure 5. Performance of SBA and effector's gulp gripper mode. (a) The pressure-length relationship of SBA and the fitting curve. (b) The grasp range and (c) force of the facet-effector. (d) Working as the MFG, the adaptability for grasping various objects is tested.

$$\begin{cases} l = 5.0844p + 138.7415, p < 0; \\ l = 1.0355p + 139.1741, p \geq 0. \end{cases} \quad (11)$$

C. MFG Performance

The facet-effector can function as a gulp gripper. Its grasping range, gripping capability, and holding force are evaluated. For the grasping range assessment, three bottom SBAs are arranged on separate sliding tracks at 120° intervals. They are interconnected by air tubes, with pressure measured. Additionally, distance is measured using the laser sensor. By subtracting the deformed value from the initial distance and converting the diameter from the circumscribed circle to the inscribed circle, the grasping range is obtained as 36.3-109.1 mm. For gripping force tests, a force transducer is positioned on the central platform. The force induced by the contractions of the SBAs is applied at the contact point of the connector, directed towards the circle's center, resulting in a measured holding force of approximately 7 N.

The gripper's capability to grasp objects of various softness, sizes, shapes, and weights is tested. Five commonly found laboratory objects are selected: a cup with a handle (86 mm in diameter), a small ball (37 mm in diameter), an electric screwdriver, an irregularly shaped batfish toy, and a 1kg weight. The image recordings demonstrated the gripper successfully securing all five objects, as shown in Fig. 5(d).

D. MFA Performance

The effector's movements and payload are tested in the MFA mode. Its angles are recorded by the IMU, displacements are measured by laser sensors, and the pressure input is captured by pressure sensors. The motions of each DOF are depicted in Fig. 6(a). Apart from the Z-axis translation, the movements of the other five DOFs exhibit symmetry in opposite directions. The recorded range data for these movements are presented in Table II.

To validate the kinematic model, inputs of pressurization at 7.5 kPa and depressurization at -7.5 kPa are applied. Model and experimental results are plotted in Fig. 6(b), depicting the relationship between the input pressure and the output motions in each DOF. In this representation, all the actuators are connected together in Z-axis translation, with the abscissa representing the unified pressure, while the abscissa for the other cases represents the pressure difference between connected actuators in two groups. In general, the model data exceeds the measured data. This could be attributed to the strong coupling observed in the motions of the SBAs, wherein air pressure not only contributes to elongation but also resists the forces generated within the coupling.

TABLE II. RANGE OF MOTIONS

Translations	Range	Rotations	Range
X	-43.7 ~ 40.7 mm	X	-28.0 ~ 26.3°
Y	-54.5 ~ 55.1 mm	Y	-29.3 ~ 32.1°
Z	-67.1 ~ 29.4 mm	Z	-35.4 ~ 35.9°

In the torsional output test (Fig. 6(c)), torque sensors are fixed between the moving panel and the fixed platform to record torque and pressure. The robot demonstrates the capability to generate a torque of 2.7 Nm.

E. Demonstrations of MFE robot

Here, demonstrations are presented to illustrate the multifaceted collaboration functionality of the robot. In diverse manufacturing settings, robots are commonly employed for a range of complex tasks, from assembly to processing and positioning.

In the first task, the robot showcases its ability to manipulate objects from distinct orientations while stationed at a fixed position, as depicted in Fig. 7. A red bolt is positioned directly above the platform, a blue bolt is in front, and a green bolt is to the left. The robot stabilizes itself by gripping onto a protrusion on the platform's bottom. The top, front, and left-side effectors successfully unscrew the bolts through the cycle

of grabbing, twisting, releasing, and returning, demonstrating the robot's versatility in completing tasks effectively from the same location.

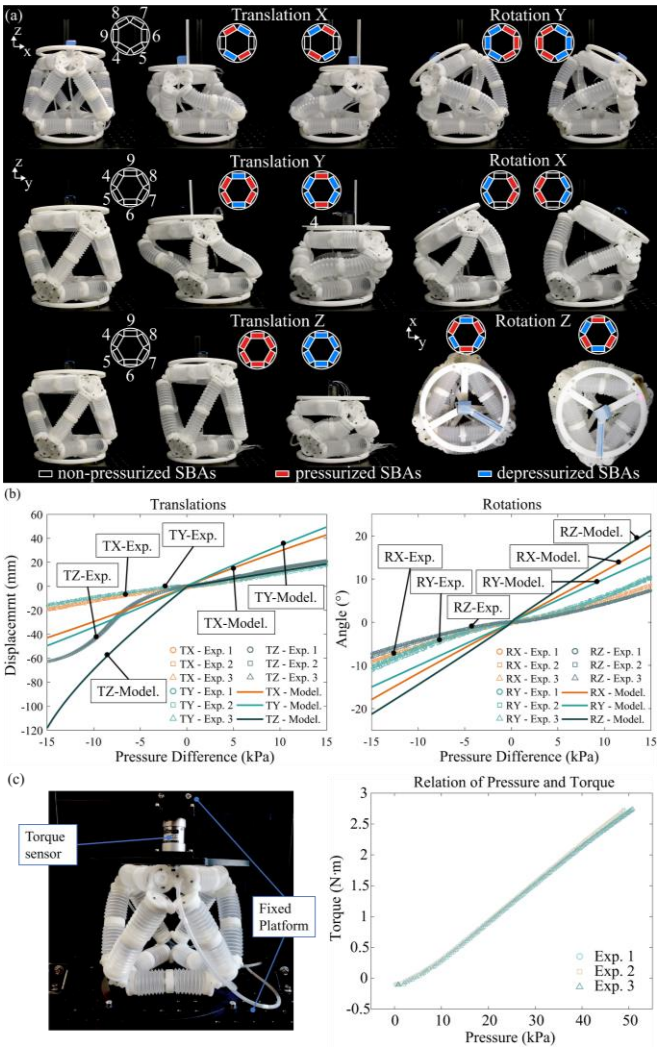

Figure 6. Performance of effector's parallel arm mode. (a) The actuation scheme and movements are illustrated with numbers around the circle corresponding to the SBAs in the body. (b) Experiment and modeling data comparison. (c) Relation of pressure and torque.

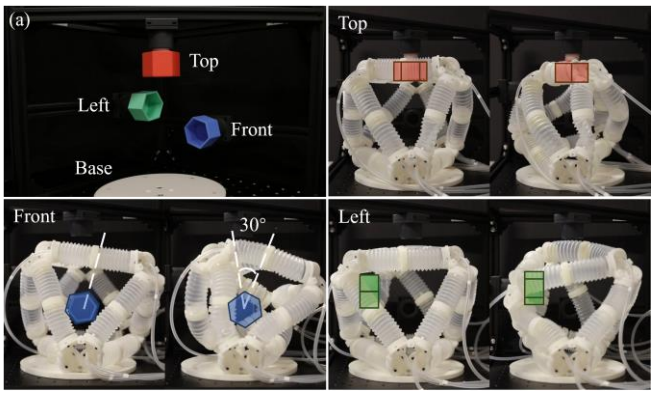

Figure 7. Demonstration of the MFE robot. The robot unscrews bolts from distinct orientations while stationed at a fixed position. It performs a cycle of grabbing, twisting, releasing, and returning, showcasing its multifaceted manipulation capabilities.

Application scenarios typically occur in complex and dynamic environments, such as post-disaster rescue missions, and involve tasks such as searching for trapped individuals. It requires robots to perform tasks like climbing, traversing rugged terrains, and overcoming obstacles to implement rescue operations while minimizing risks to personnel. Here, the second task demonstrates the robot's maneuverability in a complex environment with spatial extruding obstacles, as shown in Fig. 8. The robot achieves 3D climbing in such intricate and interwoven terrains by coordinately adjusting its opposite facet-effectors and alternately expanding and contracting them for grabbing, repositioning and moving. From start to end, the robot grabbed and repositioned four times to descend a 20cm distance and travel a 135° angular displacement from the left-upper position to the right-lower position, and avoided the spatial obstacles.

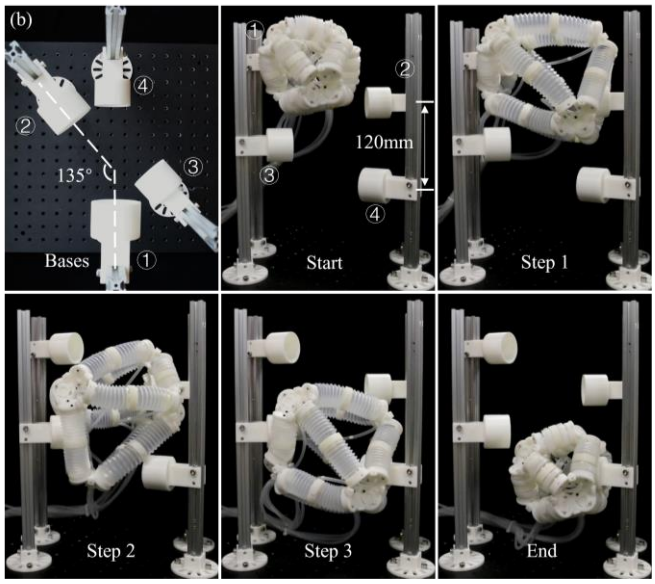

Figure 8. Demonstration of the MFE robot. In a challenging environment with spatially protruding obstacles, the robot achieves 3D climbing in the intricate and interwoven terrains by coordinately adjusting its opposite facet-effectors and alternately expanding and contracting them for grabbing, repositioning, and moving.

V. Conclusion

In this work, we introduce a novel approach to the design of soft robots through the implementation of 2D triangular Multi-Facet-Effectors on the discrete surfaces of the octahedral configuration, granting the MFE robot with identical and interchangeable functions of each facet. Experiments are conducted on two functional modes of the effector, i.e., the gulp gripper (MFG) and parallel arm (MFA). When in MFG mode, the robot exhibits the capability to grasp objects within a diameter range of 36.3-109.1 mm, with the most significant holding force of approximately 7 N. This gripping stability extends to objects of various shapes, rigidities, and weights. The six-DOF motions as MFA are investigated, showing symmetric behavior in five DOFs. Translations along the X and Y directions reach approximately 42.2 mm, while translation in the Z direction spans from -67.1 to 29.4 mm. Unidirectional rotation angles around the X, Y, and Z axes are approximately 27.2°, 30.7°,

and 35.7°, respectively. The established kinematic model for the MFA is validated through experiments. The work's advantages lie in collaboration between effectors and multidirectional function reuse, showcasing a balanced performance in both grasping and motion functions. The repetitive-facet configuration allows for identical motion and functionality across each facet, enabling the achievement of versatile capabilities without the need for intricate and specific designs. The proposed MFE soft robot demonstrates excellent operational capabilities and mobility in 3D spaces. Coordinated actions among MFE empower the robot to execute diverse tasks, showcasing its capability for multi-facet manipulations and climbing on complex terrains. The research holds potential contributions to the development of soft robots designed for multifunctional applications in unstructured environments.

Future work involves further refinement of the design to ensure alignment between the model and the prototype, deriving inverse kinematics models for feedback control, and explorations of more effective collaboration between effectors for various applications.

REFERENCES

[1] Yasa, O., Y. Toshimitsu, M.Y. Michelis, et al., "An Overview of Soft Robotics", Annual Review of Control, Robotics, and Autonomous Systems 6(1), 2023, pp. 1–29.

[2] Rus, D., and M.T. Tolley, "Design, fabrication and control of soft robots", Nature 521(7553), 2015, pp. 467–475.

[3] Chen, Xiaoqian, et al. "A review of soft manipulator research, applications, and opportunities." Journal of Field Robotics 39.3 (2022): 281-311.

[4] Polygerinos, P., Z. Wang, K.C. Galloway, R.J. Wood, and C.J. Walsh, "Soft robotic glove for combined assistance and at-home rehabilitation", Robotics and Autonomous Systems 73, 2015, pp. 135–143.

[5] Liu, S., Y. Zhu, Z. Zhang, et al., "Otariidae-Inspired Soft-Robotic Supernumerary Flippers by Fabric Kirigami and Origami", IEEE/ASME Transactions on Mechatronics 26(5), 2021, pp. 2747–2757.

[6] Tang, Kailuan, et al. "A Strong Underwater Soft Manipulator with Planarly-bundled Actuators and Accurate Position Control." IEEE Robotics and Automation Letters (2023).

[7] Fang, J., Y. Zhuang, K. Liu, et al., "A Shift from Efficiency to Adaptability: Recent Progress in Biomimetic Interactive Soft Robotics in Wet Environments", Advanced Science 9(8), 2022, pp. 2104347.

[8] Zhou, L., L. Ren, Y. Chen, S. Niu, Z. Han, and L. Ren, "Bio-Inspired Soft Grippers Based on Impactive Gripping", Advanced Science 8(9), 2021, pp. 2002017.

[9] Wang, Zheng, et al. "The next-generation surgical robots." Surgical Robotics (2018): 1.

[10] Kang, Rongjie, et al. "Design of a pneumatic muscle based continuum robot with embedded tendons." IEEE/ASME Transactions on Mechatronics 22.2 (2016): 751-761.

[11] Shintake, J., V. Cacucciolo, D. Floreano, and H. Shea, "Soft Robotic Grippers", Advanced Materials 30(29), 2018, pp. 1707035.

[12] Salerno, Marco, et al. "A novel 4-DOFs origami enabled, SMA actuated, robotic end-effector for minimally invasive surgery." 2014 IEEE international conference on robotics and automation (ICRA). IEEE, 2014.

[13] Liu, Q., X. Gu, N. Tan, and H. Ren, "Soft Robotic Gripper Driven by Flexible Shafts for Simultaneous Grasping and In-Hand Cap Manipulation", IEEE Transactions on Automation Science and Engineering 18(3), 2021, pp. 1134–1143.

[14] Xie, Z., F. Yuan, J. Liu, et al., "Octopus-inspired sensorized soft arm for environmental interaction", Science Robotics 8(84), 2023, pp. eadh7852.

[15] Dai, Jian S., Matteo Zoppi, and Xianwen Kong, eds. Advances in reconfigurable mechanisms and robots I. London: Springer, 2012.

[16] Aimedee, F., et al. "Systematization of morphing in reconfigurable mechanisms." Mechanism and machine theory 96 (2016): 215-224.

[17] Shah, D.S., J.P. Powers, L.G. Tilton, S. Kriegman, J. Bongard, and R. Kramer-Bottiglio, "A soft robot that adapts to environments through shape change", Nature Machine Intelligence 3(1), 2021, pp. 51–59.

[18] Tan, Qinlin, et al. "Underwater crawling robot with hydraulic soft actuators." Frontiers in Robotics and AI 8 (2021): 688697.

[19] Zagal, J.C., C. Armstrong, and S. Li, Deformable Octahedron Burrowing Robot, 2012.

[20] Singh, G., S. Patiballa, X. Zhang, and G. Krishnan, "A Pipe-Climbing Soft Robot", 2019 International Conference on Robotics and Automation (ICRA), (2019), 8450–8456.

[21] Liu, S., J. Liu, K. Zou, et al., "A Six Degrees-of-Freedom Soft Robotic Joint With Tilt-Arranged Origami Actuator", Journal of Mechanisms and Robotics 14(060912), 2022.

[22] Liu, Jianhui, et al. "Vertebraic Soft Robotic Joint Design With Twisting and Antagonism." IEEE Robotics and Automation Letters 7.2 (2021): 658-665.

[23] Yin, A., H.-C. Lin, J. Thelen, B. Mahner, and T. Ranzani, "Combining Locomotion and Grasping Functionalities in Soft Robots", Advanced Intelligent Systems 1(8), 2019, pp. 1900089.

[24] Cianchetti, M., M. Calisti, L. Margheri, M. Kuba, and C. Laschi, "Bioinspired locomotion and grasping in water: the soft eight-arm OCTOPUS robot", Bioinspiration & Biomimetics 10(3), 2015, pp. 035003.

[25] Liu, Sicong, et al. "Deployable prismatic structures with origami patterns." International Design Engineering Technical Conferences and Computers and Information in Engineering Conference. Vol. 46377. American Society of Mechanical Engineers, 2014.

[26] Wharton, Peter, et al. "Tetraflex: A Multigait Soft Robot for Object Transportation in Confined Environments." IEEE Robotics and Automation Letters (2023).

[27] Fang, Zhonggui, et al. "Omnidirectional compliance on cross-linked actuator coordination enables simultaneous multi-functions of soft modular robots." Scientific Reports 13.1 (2023): 12116.

[28] Guan, Q., L. Liu, J. Sun, et al., "Multifunctional Soft Stackable Robots by Netting–Rolling–Splicing Pneumatic Artificial Muscles", Soft Robotics 10(5), 2023, pp. 1001–1014.

[29] Usevitch, N.S., Z.M. Hammond, M. Schwager, A.M. Okamura, E.W. Hawkes, and S. Follmer, "An untethered isoperimetric soft robot", Science Robotics 5(40), 2020, pp. eaaz0492.

[30] Zhou J, Chen Y, Chen X, et al. A proprioceptive bellows (PB) actuator with position feedback and force estimation[J]. IEEE Robotics and Automation Letters, 2020, 5(2): 1867-1874.

[31] Chen, Xiaojiao, Yaoxin Guo, Dehao Duanmu, Jianshu Zhou, Wei Zhang, and Zheng Wang. "Design and modeling of an extensible soft robotic arm." IEEE Robotics and Automation Letters 4, no. 4 (2019): 4208-4215.

[32] Tian, Wei-Hang, et al. "Development of a tetrahedral-shaped soft robot arm as a wrist rehabilitation device using extension type flexible pneumatic actuators." Journal of Robotics and Mechatronics 32.5 (2020): 931-938.

[33] Zhao, Ziming, et al. "Envelop-Climbing Locomotion Planning and Capability Analysis of a Deformable Tetrahedron Rolling Robot." IEEE Robotics and Automation Letters (2023).